AN IMAGE IS WORTH TEN THOUSAND WORDS: VERBOSE-TEXT INDUCTION ATTACKS ON VLMS

Zhi Luo, Zenghui Yuan *

Huazhong University of Science and Technology {zhi_luo,zenghuiyuan}@hust.edu.cn

Wenqi Wei

Fordham University wengiwei@fordham.edu

Daizong Liu

Wuhan University daizongliu@whu.edu.cn

Pan Zhou

Huazhong University of Science and Technology panzhou@hust.edu.cn

ABSTRACT

With the remarkable success of Vision-Language Models (VLMs) on multimodal tasks, concerns regarding their deployment efficiency have become increasingly prominent. In particular, the number of tokens consumed during the generation process has emerged as a key evaluation metric. Prior studies have shown that specific inputs can induce VLMs to generate lengthy outputs with low information density, which significantly increases energy consumption, latency, and token costs. However, existing methods simply delay the occurrence of the EOS token to implicitly prolong output, and fail to directly maximize the output token length as an explicit optimization objective, lacking stability and controllability. To address these limitations, this paper proposes a novel verbose-text induction attack (VTIA) to inject imperceptible adversarial perturbations into benign images via a two-stage framework, which identifies the most malicious prompt embeddings for optimizing and maximizing the output token of the perturbed images. Specifically, we first perform adversarial prompt search, employing reinforcement learning strategies to automatically identify adversarial prompts capable of inducing the LLM component within VLMs to produce verbose outputs. We then conduct vision-aligned perturbation optimization to craft adversarial examples on input images, maximizing the similarity between the perturbed image's visual embeddings and those of the adversarial prompt, thereby constructing malicious images that trigger verbose text generation. Comprehensive experiments on four popular VLMs demonstrate that our method achieves significant advantages in terms of effectiveness, efficiency, and generalization capability.

1 Introduction

In recent years, Vision-Language Models (VLMs) have advanced rapidly, demonstrating strong performance in multimodal tasks such as image captioning (Wang et al., 2021; Li et al., 2022), visual question answering (Liu et al., 2023b; Dai et al., 2023), and visual reasoning (Zhu et al., 2023; Cheng et al., 2024). However, these achievements are largely driven by scaling models to billions of parameters, which renders the model's deployment highly resource-intensive (Zhang et al., 2024a). With the accelerating commercialization of VLMs, many service providers offer inference services for users through APIs, commonly under token-based billing schemes. This raises a critical challenge for practical deployment, which is to ensure accurate and efficient inference while suppressing redundant token generation.

^{*}Equal contribution

Most state-of-the-art VLMs adopt modular architectures in which an intermediate layer connects the visual encoder and Large Language Models (LLMs) (Yin et al., 2024). The visual encoder and intermediate layer jointly process the image to extract visual embeddings, which are then combined with the textual embeddings of prompts for response generation by the LLMs. Due to the autoregressive nature of LLMs, each generated token requires a forward pass, and the token is subsequently fed back as input for the next steps (Cao et al., 2023). As the token sequence grows, the computational cost of each forward pass increases accordingly. Such characteristics expose VLMs to a new type of security threat (Gao et al., 2024a;b): adversaries can design malicious images that induce the model to generate excessively long outputs. Such behavior not only inflates inference energy consumption and latency, severely degrading server responsiveness, but also substantially increases user costs under token-based pricing. As illustrated in Figure 1, the inference time increases with the number of generated tokens. When adversarial perturbations remain visually imperceptible, the stealth and practical risk of these attacks become even more severe.

Prior works (Shumailov et al., 2021; Chen et al., 2022b) have investigated increasing inference energy consumption and latency by adding perturbations to images, but these methods mainly target image-classification models (e.g., ResNet) or small-scale image-to-text models (e.g., ResNet+RNN) and do not readily transfer to modern VLMs. Recent studies (Gao et al., 2024a;b) on VLMs have focused on prolonging outputs by delaying the occurrence of the EOS token: their core idea is to decrease the probability of EOS in the next-step distribution and use that signal to compute gradients for optimizing image perturbations. However, this approach relies solely on the probability distribution obtained from a single forward pass of the image and input text through the VLM, therefore cannot capture the complete information

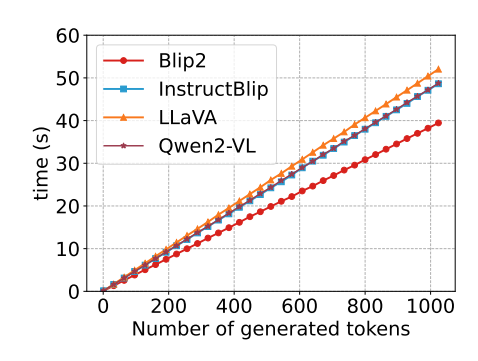


Figure 1: The relationship between the time consumed in a single inference and the number of generated tokens.

of the subsequent autoregressive generation process. That is because LLMs generate autoregressively, later outputs are highly context-dependent and thus difficult to predict or control. Consequently, adversarial images optimized using single-pass information often lack stability and controllability in their final attack effectiveness. This limitation raises a key question: **can we directly use the VLM's output length as the optimization objective when optimizing an adversarial image for verbose text, thereby improving the stability and controllability of adversarial methods?**

To address these limitations, in this paper, we propose a novel redundancy-inducing VLM attack, termed Verbose-Text Induction Attack (VTIA). This attack method adopts a two-stage decoupling strategy that explicitly learn the most malicious prompt embedding and maximizes the output token numbers of the perturbed images. In particular, it proceeds in two steps: 1) Adversarial Prompt Search: we train an attacker LLM using reinforcement learning to optimize the generation of a malicious prompt, avoiding the non-differentiability of directly maximizing output token length. The embedding of this prompt, when inserted after the visual embeddings, can trigger the LLM within the VLM to produce excessively long outputs; 2) Vision-Aligned Perturbation Optimization: based on the similarity between the malicious prompt embedding and visual embeddings, gradients are computed to perturb the input image and obtain adversarial examples. This stage operates entirely independently of the target VLM's textual module, thereby avoiding the substantial overhead of repeatedly invoking large LLMs during iterative optimization. In this manner, our attack can effectively prolong the VLM's output. The main contributions of this work are as follows:

- We propose a novel verbose-text induction attack on VLMs, capable of generating adversarial images while accounting for subsequent outputs with explicit token-aware designs, thereby advancing security research on inducing verbose text generation in VLMs.
- We design a two-stage attack framework, which firstly searches for an adversarial prompt through reinforcement learning, and then uses it to optimize adversarial images with the defined similarity loss and standard deviation loss.

• We apply our method to four mainstream VLMs (Blip2, InstructBlip, LLaVA, Qwen2-VL) and evaluate it on the MS-COCO dataset. Experimental results show that the generated adversarial images can induce these models to produce token counts that are 121.90×, 87.19×, 9.44×, and 6.48× longer than those generated from the original images.

2 RELATED WORK

2.1 VLMs

Currently, mainstream VLMs consist of two key parts, i.e., textual and visual components. Early models such as CLIP (Radford et al., 2021), BLIP (Li et al., 2022), and ALIGN (Jia et al., 2021) employed both visual encoders and text encoders, aligning image and text embeddings through contrastive learning. Newer generations of models (e.g., Blip2 (Li et al., 2023), InstructBlip (Dai et al., 2023), MiniGPT (Zhu et al., 2023), LLaVA (Liu et al., 2023b), Qwen2-VL (Wang et al., 2024)) typically no longer include a standalone text encoder. Instead, they rely on LLMs, such as OPT (Zhang et al., 2022), LLaMA (Touvron et al., 2023), Vicuna (Chiang et al., 2023), and Qwen (Bai et al., 2023), for text understanding, while integrating visual inputs through projection layers or cross-attention mechanisms. This trend reflects a growing shift toward leveraging the capabilities of LLMs, rather than relying solely on visual components, to support more flexible and advanced multimodal reasoning and generation tasks.

2.2 ENERGY-LATENCY ATTACKS

Prior research (Chen et al., 2022a; Hong et al., 2020; Liu et al., 2023a; Chen et al., 2023; Zhang et al., 2024b; Dong et al., 2024) has investigated how to construct adversarial inputs to degrade the model inference efficiency. Shumailov et al. (2021) analyzed both language and vision models; in the case of vision models, the focus was on classification architectures such as ResNet (He et al., 2016), DenseNet (Huang et al., 2017), and MobileNet (Howard et al., 2017). The approach involved designing adversarial image inputs that increase activation values across layers. Higher activation density prevents hardware from skipping certain computations, thereby increasing energy consumption. However, this work did not consider multimodal models. Chen et al. (2022b) examined the efficiency of Neural Image Caption Generation (NICG) models, proposing to delay the occurrence of EOS tokens while disrupting token dependencies, thereby generating longer sequences. This increases the number of decoder calls and reduces inference efficiency. Nonetheless, their studied architectures (MobileNets+LSTM, ResNet+RNN) differ significantly from the Transformer-based architectures used in current mainstream VLMs. To induce VLMs to generate longer responses, Gao et al. (2024a) and Gao et al. (2024b) proposed three strategies: 1) lowering the probability of EOS token generation to delay its appearance; 2) enhancing output uncertainty to encourage predictions that deviate from the original token order and pay more attention to alternative candidate tokens; and 3) improving the diversity of hidden states across generated tokens to explore a broader output space, thereby further weakening original output dependencies. However, these works typically proxy increased output verbosity by manipulating the EOS token probability rather than treating token length as an explicit optimization objective. Given the autoregressive nature of current models, where outputs serve as inputs for subsequent steps, and the fact that the loss function is constructed solely from distributions obtained in a single forward pass, the attack effectiveness of such adversarial samples remains difficult to guarantee.

3 Preliminaries

3.1 STRUCTURE OF VLMs

Existing state-of-the-art VLMs, such as Blip2 (Li et al., 2023), InstructBLIP (Dai et al., 2023), LLaVA (Liu et al., 2023b), and Qwen2-VL (Wang et al., 2024), generally consist of a visual encoder $\mathcal E$ and a pretrained LLM $\mathcal F$. To bridge the two components, an intermediate module $\mathcal M$ is required. For example, in InstructBLIP, this module consists of a Q-Former and a fully connected layer. While in LLaVA, it is implemented as a linear layer that maps the visual features extracted by the visual encoder into the word embedding space.

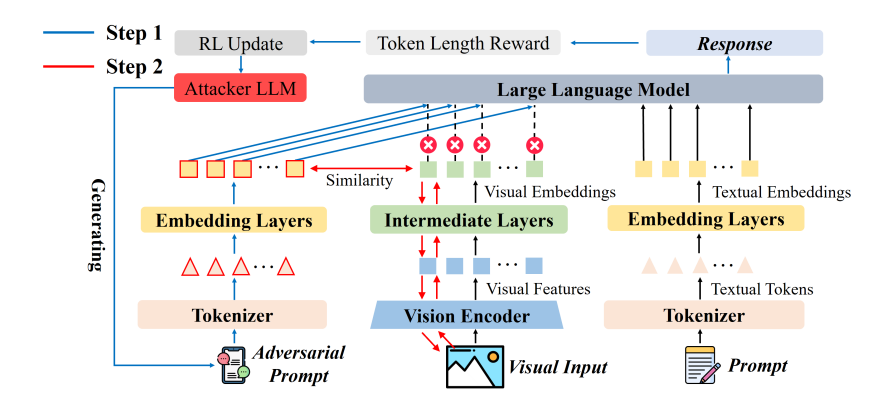


Figure 2: Flowchart of VTIA. Step 1: Adversarial prompt search; Step 2: Vision-aligned perturbation optimization.

Given an input image x, the visual encoder first encodes the input image as visual features $Z_v = \mathcal{E}(x)$. Subsequently, the intermediate module projects the visual features into visual embeddings $H_v = \mathcal{M}(Z_v)$, which has the dimension of m (i.e., the visual token number of the VLM). And for the input prompt c, it is first processed by tokenizer \mathcal{T} into a textual token sequence $S_t = \mathcal{T}(c) = \{s_1, s_2, \cdots, s_n\}$ of length n. Then S_t is projected by the embedding layers \mathcal{D} into textual embeddings $H_t = \mathcal{D}(S_t)$. Finally, the visual embedding H_v is concatenated with the textual embedding H_t to form the initial sequence, and then fed into the LLM for content generation in an autoregressive manner. Represent the initial sequence as $H_v \oplus H_t$, it is fed into the LLM \mathcal{F} , which produces a probability distribution over the next token. By sampling from this distribution, the next token is obtained and appended to the original sequence, which serves as the input for the next decoding step of the LLM. Formally, the response of the LLM can be denoted as $y = \mathcal{F}(\mathcal{M}(\mathcal{E}(x) \oplus \mathcal{D}(\mathcal{T}(c)))$. The generation process terminates under either of the following conditions: 1) The generated token is an EOS token in a given step. 2) The number of generated tokens reaches a predefined maximum value.

3.2 THREAT MODEL

Attacker's Knowledge. We consider a gray-box attack setting in which the attacker has access to the model structure of the target VLM f, as well as the parameters of the visual encoder \mathcal{E} and the intermediate module \mathcal{M} . While the attacker does not require the LLM's parameters.

Attacker's Goal. The attacker aims to generate an adversarial image that induces the VLM to produce maximally verbose responses. Such responses increase inference costs, including computational and energy consumption, latency, and monetary expenses.

Attacker's Constraint. The magnitude of the perturbations applied to the image is bounded by a predefined l_p norm, ensuring the stealthiness of the attack.

4 ATTACK METHOD

4.1 INSIGHT OF VTIA

The goal of our attack is to find an adversarial perturbation δ that, when added to a clean image x, yields a perturbed image $x^* = x + \delta$ that causes the victim VLM f to produce the output g with maximal token length. Formally, let $len(\cdot)$ denotes the token-count operator and let f represents the target VLM, we aim to solve

$$\max_{\delta} \mathbb{E}_{y = \mathcal{F}(\mathcal{M}(\mathcal{E}(x^*) \oplus \mathcal{D}(\mathcal{D}(c)))} [\text{len}(y)], \tag{1}$$

$$\text{s.t. } ||x^* - x||_p \le \epsilon, \tag{2}$$

where $||\cdot||_p$ is the l_p norm constraint and ϵ indicates the perturbation magnitude. However, the above problem cannot be solved directly because len(y) is not differentiable with respect to δ . Therefore,

Algorithm 1 Process of vision-aligned perturbation optimization

- 1: **Input:** Origin images x, the perturbation magnitude ϵ , step size lr, optimization iterations T and momentum value μ ;
- 2: **Output:** An adversarial image x^* with $||x^* x||_p \le \epsilon$.
- 3: $g_0 = 0, x_0^* = x$;
- 4: **for** t = 0 to T 1 **do**
- 5: Input x_t^* to VLM and calculate the loss \mathcal{L}_{total} according to Equation (8);
- 6: Update g_{t+1} by:

$$g_{t+1} = \mu \cdot g_t + \frac{\nabla \mathcal{F}(x_t^*)}{\|\nabla \mathcal{F}(x_t^*)\|_1};$$
(4)

7: Update x_{t+1}^* by:

$$x_{t+1}^* = x_t^* - lr \cdot sign(g_{t+1}); \tag{5}$$

- 8: end for
- 9: **return** x_T^*

we design two steps to achieve the attack goal: 1) **Adversarial prompt search**: We directly construct the token length of the VLM's response as the reinforcement learning reward. To reduce the search space, we optimize an attacker LLM to produce discrete textual prompts whose embeddings replace image embeddings, thereby inducing the targeted adversarial behavior. 2) **Vision-aligned perturbation optimization**: We split the optimized adversarial prompt into token slices and optimize an objective that jointly penalizes slice—image embedding dissimilarity and standard deviation, and apply backpropagation to optimize and obtain the adversarial image. Our proposed VTIA can capture the VLM's output during the adversarial prompt search stage, compensating for the limitation of existing approaches (Gao et al., 2024a;b), which cannot observe the subsequent autoregressive generation process when creating adversarial images. Figure 2 illustrates the workflow of our proposed attack method.

4.2 ADVERSARIAL PROMPT SEARCH

In the first step, we optimize an attacker LLM \mathcal{F}^* to produce adversarial prompts c^* . Then c^* is tokenized and projected into textual embeddings H_t^* , and is used to replace the visual embedding H_v of the target VLM. The search objective is to maximize the VLM's output length (i.e., induce the most verbose responses). This problem can be naturally solved through the following formulation of reinforcement learning:

$$\arg \max_{\mathcal{F}^*} \mathbb{E}_{y = \mathcal{F}(\mathcal{D}(\mathcal{T}(c^*) \oplus \mathcal{D}(\mathcal{T}(c))}[\text{len}(y)], \tag{3}$$

which takes the token length of the response as the reward. We use \mathcal{F}^* to generate an adversarial prompt c^* containing k tokens, and slice its corresponding textual embedding H_t^* according to the visual token number m corresponding to the target VLM. Specifically, we set the dimension corresponding to the sliced embedding $H_t^*[k']$ to an integer k' that is divisible by m (e.g., when m is 32, k' can be 4), corresponding to the vector of the first k' dimensions of H_t^* . Subsequently, we repeat $H_t^*[k']$ for m/k' times and replace it with the model's visual embeddings to generate the response. We use the Proximal Policy Optimization (PPO) strategy to optimize f^* according to the objectives in Equation (3). By repeating this process, one can eventually identify an adversarial prompt that induces the LLM to generate a token count reaching the predefined upper bound.

4.3 VISION-ALIGNED PERTURBATION OPTIMIZATION

In order to get the adversarial image x^* , we optimize the perturbation δ through vision-aligned perturbation optimization based on the generated adversarial prompt c^* . Let the visual embedding of the adversarial image be represented as $H_v^* = [v_1, v_2, v_3, \ldots, v_m]$, where m denotes the number of visual tokens, and v_i represents the visual embedding vector. Correspondingly, the concatenated embedding of the adversarial prompt slice is represented as $[H_t^*[:k']_1, H_t^*[:k']_2, \cdots, H_t^*[:k']_{m/k'}] = [t_1, t_2, t_3, \ldots, t_m]$, where t_i denotes the text embedding vector. Since the concatenated adversarial prompt embedding is fixed after step one, we need to optimize a perturbation δ , so that the adversarial image's embedding closely matches the prompt's per-token embeddings, thereby reproducing

Table 1: Key information of the large models used in the experiments, including model scale (number of parameters), type of visual module, the LLM employed, and the number of visual tokens.

Model	Parameters	Vision Encoder	LLM	Visual token number
Blip2	2.7B	ViT-B/L/g	OPT	32
InstructBlip	7B	ViT	Vicuna	32
LLaVA-1.5	7B	CLIP ViT-L/14	Vicuna	576
Qwen2-VL	2B	EVA-CLIP ViT-L	Qwen-2	dynamic

the same verbose behavior. Therefore, it is necessary to maximize the cosine similarity between v_i and t_i . Upon this, we define the similarity loss \mathcal{L}_{sim} as:

$$\mathcal{L}_{sim} = \frac{1}{m} \sum_{i=1}^{m} \cos(\mathcal{M}(\mathcal{E}(x+\delta)[i], t_i)), \tag{6}$$

which is the mean cosine similarity between the visual and textual embeddings. However, if only \mathcal{L}_{sim} is used as the loss term, the optimization process may lead to a situation where some (v_i, t_i) pairs achieve sufficient optimization, while others (v_j, t_j) remain under-optimized. This imbalance can result in adversarial images with suboptimal attack performance. To address this issue and ensure that each (v_i, t_i) pair is adequately optimized, we introduce a standard deviation term into the loss function. Then define \mathcal{L}_{std} as:

$$\mathcal{L}_{std} = \sqrt{\frac{1}{m} \sum_{i=1}^{m} \left(\cos(\mathcal{M}(\mathcal{E}(x+\delta)[i], t_i) - \mathcal{L}_{sim} \right)^2},$$
 (7)

which is the standard deviation of the cosine similarity between the visual and text embeddings. Based on the two loss terms, the optimization objective is formulated as:

$$\min_{x^*} \mathcal{L}_{total} = -\mathcal{L}_{sim} + \alpha \cdot \mathcal{L}_{std}, \quad \text{s.t. } ||x^* - x||_p \le \epsilon,$$
 (8)

where α is a hyperparameter that balances the two losses. Furthermore, we use a momentum μ to control the update of x^* . The specific process is shown in Algorithm 1.

5 EXPERIMENTS

5.1 EXPERIMENTAL SETUPS

Models and datasets. This study employs four open-source models: Blip2, InstructBlip, LLaVA, and Qwen2-VL. Table 1 presents detailed information about these models. Unlike the first three, Qwen2-VL's number of visual tokens varies with image resolution. Consequently, prior to feeding images into Qwen2-VL, we uniformly resize them to 336×336 , resulting in 144 visual tokens. In the Visual Question Answering task, Blip2 and InstructBlip use the language prompt "Please describe this picture. Answer:", whereas LLaVA and Qwen2-VL utilize a conversational template with the text portion "Please describe this picture." We randomly select 100 images from the MS-COCO dataset as experimental samples.

Baselines and setups. As a baseline, we use the original images, images with added random noise, and verbose images. The perturbation magnitude is set to $\epsilon=8$ under an ℓ_{∞} constraint. For both the verbose images and our method, we employ the PGD algorithm with 5,000 iterations. For the verbose images, the step size and momentum are set to 0.0039 and 0.9, respectively, as reported in the original source. For our method, the weight is $\alpha=0.8$, the step size (lr) is 0.0022, and the momentum is $\mu=0.9$. In the reinforcement-learning component, we use PPO; the attacker LLM is GPT-2 XL with a learning rate of 1.46×10^{-5} and a clip range of 0.3. After the attacker LLM generates a token sequence, we extract a slice and repeat that slice until it matches the number of visual tokens. For example, if the slice contains two tokens and the VLM (e.g., InstructBLIP) has 32 visual tokens, the slice is repeated 32/2 times to match the visual-token count. For all VLMs

Table 2: Comparison of the text-generation induction effects (e.g., number of generated tokens) of the original images, images with added random noise, verbose images, and VTIA on Blip2, InstructBLIP, LLaVA, and Qwen2-VL.

VLM model	Method	Average length	Average length / max length	Extra long rate (%)
Qwen2-VL	Origin	158.14	0.1544	1
	Noise	145.04	0.1416	0
	Verbose Images	809.01	0.7900	70
	VTIA (ours)	1024	1.0000	100
LLaVA	Origin	108.38	0.1058	0
	Noise	108.58	0.1060	0
	Verbose Images	518.61	0.5065	42
	VTIA (ours)	1024	1.0000	100
	Origin	11.63	0.0114	0
InstructBlip	Noise	11.37	0.0111	0
	Verbose Images	1003.86	0.9803	98
	VTIA (ours)	1014	0.9902	99
Blip2	Origin	8.4	0.0082	0
	Noise	8.32	0.0081	0
	Verbose Images	933.19	0.9113	91
	VTIA (ours)	1024	1.0000	100

used in our experiments, the maximum number of generated tokens is set to 1024, and generation is performed using greedy decoding.

Evaluation metrics. We record the number of tokens generated per image and compute the average generation length (Average length) across the 100 images, as well as the proportion of samples producing more than 1000 tokens (Extra long rate).

5.2 Main Results

Table 2 presents the experimental results on four models. It can be seen that the number of generated tokens produced by images with added random noise is similar to that of the original images, indicating that simply adding random noise is insufficient to trigger verbose outputs from VLMs; achieving verbose outputs requires carefully designed image perturbations. Although the verbose images method can generate malicious images that induce verbose text, its effectiveness remains inferior to our proposed method. The performance gap is especially pronounced for the two more recent models, LLaVA and Qwen2-VL (Gao et al. (2024a) did not evaluate these two models), which further demonstrates the advantage of the "search adversarial prompt first, then optimize image perturbations" strategy.

Figure 3 displays the original images and the adversarial images, and compares the cosine-similarity distributions between their visual embeddings and the embeddings of the adversarial prompt. The results show that after applying small perturbations to the original images, the cosine similarities of most visual embeddings with their corresponding adversarial-prompt embeddings increase. Consequently, the perturbed images become semantically closer to the adversarial prompt and can trigger verbose outputs from the VLM in the same way as that prompt.

5.3 ABLATION STUDIES

We primarily investigate the effects of the \mathcal{L}_{std} term, hyperparameter α , momentum, perturbation magnitude, and the adversarial prompt on attack performance.

Impact of the \mathcal{L}_{std} **term.** Table 3 reports ablation experiments on the \mathcal{L}_{std} term and momentum. Vertical comparisons indicate that adding \mathcal{L}_{std} to the loss improves attack performance, particularly on Blip2 and InstructBlip; this improvement is more pronounced when momentum is not used. For LLaVA and Qwen2-VL, the impact of including \mathcal{L}_{std} is relatively small; moreover, when momentum

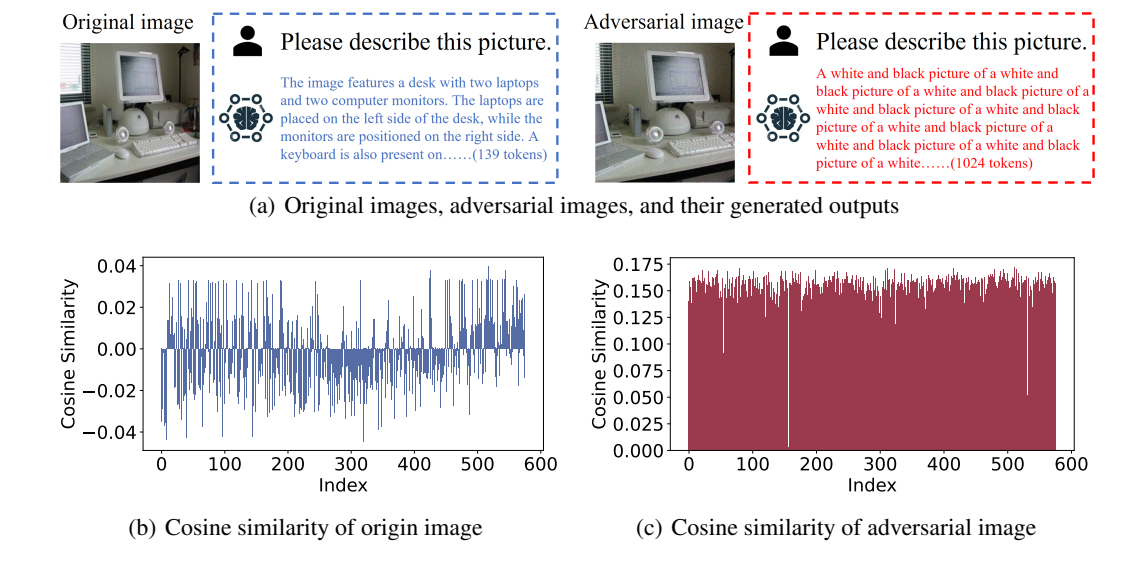


Figure 3: Examples of original images and adversarial images, together with distributions of the cosine similarity between their visual embeddings and the adversarial-prompt embeddings. The model used is LLaVA.

Table 3: Ablation experiments on the four VLMs, comparing attack performance when the \mathcal{L}_{std} term is included or excluded and when momentum is used or not.

V	LM model	\mathcal{L}_{std}	With Momentum Average length Extra long rate (%)		Without Momentum Average length Extra long rate (%)	
Q	Qwen2-VL	✓ X	1024 1024	100 100	1024 1010.75	100 98
	LLaVA	У Х	1024 1023.76	100 100	1021.31 1023.81	99 100
In	nstructBlip	У Х	1014 1004.27	99 98	793.66 551.06	77 53
	Blip2	✓ X	1024 994.18	100 97	902.9 640.34	88 62
1022 1020 1017 1015 1012 1010 1007	0.0 7.5 6.0 8.5 9.0			1020 1000 4 980 9 960 9 940 9 920 9 920 9 900 880		InstructBlip Qwen2-VL

(a) Impact of α on average token length

0.0

(b) Impact of the momentum value on average token length

0.1 0.2 0.3 0.4 0.5 0.6 0.7 0.8 0.9 momentum value

Figure 4: Effect of different weights α and different momentum values on attack performance (e.g., average generated token length), shown as curves or bar charts.

1.0

0.8

is absent, adding \mathcal{L}_{std} slightly degrades LLaVA's attack performance. Two main reasons explain this phenomenon: 1) LLaVA and Qwen2-VL have far more visual tokens than Blip2 and InstructBlip; therefore, even if some visual embeddings and their corresponding adversarial prompt embeddings

Table 4: Attack performance and perceptual-quality metrics (e.g., LPIPS) under different perturbation magnitudes (e.g., 2/255, 4/255, 8/255, 16/255).

Magnitude	LPIPS	Average length	Extra long rate (%)
2/255	0.0110	380.34	36
4/255	0.0379	793	77
8/255	0.1137	1014	99
16/255	0.2190	1024	100

Table 5: Attack performance under different adversarial prompts (constructed from repeated slices); the repetition count is computed as: visual token number/slice token number

Slice length	Average length	Extra long rate (%)
2	1014	99
4	1003.91	98
8	923.44	90
16	953.55	93
32	883.48	86

are not fully optimized in terms of cosine similarity, the overall attack is less affected. When the number of visual tokens is small, such insufficiently optimized embeddings can substantially reduce attack effectiveness. 2) Introducing the \mathcal{L}_{std} term into the loss can trade off optimization for the \mathcal{L}_{sim} term when optimizing the adversarial image. This trade-off may reduce final performance, especially when the visual token count is very large (e.g., LLaVA has 576 tokens). Horizontal comparisons show that introducing momentum improves attack performance across models.

Impact of α and momentum value. In addition, Figure 4 illustrates the effects of different α values and different momentum values on attack performance. As shown in Figure 4(a), performance on InstructBLIP is optimal when $\alpha=0.6$, further indicating that an appropriate choice of α is needed to balance the optimization of \mathcal{L}_{sim} and \mathcal{L}_{std} . In contrast, on Qwen2-VL, α has little impact on attack performance, which corroborates that when the number of visual tokens is large, whether each visual embedding is fully optimized has a reduced influence on the final outcome. Figure 4(b) shows that, for InstructBLIP, attack performance increases as the momentum value grows, implying that stable optimization is necessary for generating effective adversarial images; whereas for Qwen2-VL, the momentum value has little effect, likely because a larger number of visual tokens makes the overall optimization process more stable.

Impact of ϵ . Table 4 compares the impact of the perturbation magnitude ϵ (2/255, 4/255, 8/255, 16/255) on attack performance and reports the LPIPS between adversarial and source images. The results show that attack strength increases significantly with larger perturbation magnitude, but the perturbations also become more perceptible. Therefore, in practical attacks one must trade off stealthiness and attack effectiveness and select an appropriate perturbation magnitude.

Impact of slice length. Table 5 presents the impact of different slice lengths on attack performance. The table shows that although various adversarial prompts can all induce VLMs to generate tokens up to the maximum limit, the final attack effectiveness of the resulting adversarial images still differs after the vision-aligned perturbation optimization step. Moreover, as the slice length increases, attack performance tends to decline. We attribute this mainly to the large amount of repetition and redundancy in image pixels: if an adversarial prompt contains many repeated tokens, it matches the image's information-carrying characteristics and thereby reduces the difficulty of the vision-aligned perturbation optimization.

6 Conclusion

This paper aims to construct imperceptible image perturbations that induce VLMs to produce verbose responses, thereby increasing the computational, time, and monetary costs associated with

the inference process of VLMs. To achieve this, we propose a two-stage decoupled attack, named VTIA. In stage one, we treat the VLM's generated token count as a reward and apply reinforcement learning to optimize an attacker LLM that discovers adversarial prompt embeddings. In stage two, we optimize image perturbations by the trade-off between the similarity loss and the standard deviation loss, ensuring that the visual embeddings align with the adversarial-prompt embeddings while keeping the perturbations visually imperceptible. Experiments on popular VLMs — BLIP2, InstructBLIP, LLaVA, and Qwen2-VL — show that the constructed adversarial images significantly increase the number of generated tokens while maintaining high visual stealthiness, highlighting the potential threat of such attacks in real-world deployments.

Ethics statement. This paper investigates the security vulnerabilities of VLMs by proposing a verbose-text induction attack that maliciously prolongs model outputs. Our goal is not to promote harmful usage but to highlight critical risks associated with excessive token generation, which can inflate energy consumption, increase operational costs, and impair system responsiveness. All experiments were conducted on publicly available models and datasets. No private or sensitive data was used, and no real-world deployment systems were attacked. We release our findings in the spirit of responsible disclosure, aiming to assist the community in understanding potential risks and motivating the development of more robust and cost-efficient VLMs.

Reproducibility statement. To ensure reproducibility, we provide comprehensive details of our methodology and experimental setup. Specifically, we describe the two-stage framework, including reinforcement learning strategies for adversarial prompt search and the vision-aligned perturbation optimization procedure. Hyperparameters, training configurations, and evaluation protocols are reported in the main paper and supplementary material. Experiments were conducted on four widely used VLMs with publicly available checkpoints. All code, configurations, and perturbation generation scripts will be released upon publication to facilitate verification and further research.

REFERENCES

- Jinze Bai, Shuai Bai, Yunfei Chu, Zeyu Cui, Kai Dang, Xiaodong Deng, Yang Fan, Wenbin Ge, Yu Han, Fei Huang, et al. Qwen technical report. *arXiv preprint arXiv:2309.16609*, 2023.
- Yihan Cao, Siyu Li, Yixin Liu, Zhiling Yan, Yutong Dai, Philip S Yu, and Lichao Sun. A comprehensive survey of ai-generated content (aigc): A history of generative ai from gan to chatgpt. arXiv preprint arXiv:2303.04226, 2023.
- Simin Chen, Cong Liu, Mirazul Haque, Zihe Song, and Wei Yang. Nmtsloth: understanding and testing efficiency degradation of neural machine translation systems. In *Proceedings of the 30th ACM Joint European Software Engineering Conference and Symposium on the Foundations of Software Engineering*, pp. 1148–1160, 2022a.
- Simin Chen, Zihe Song, Mirazul Haque, Cong Liu, and Wei Yang. Nicgslowdown: Evaluating the efficiency robustness of neural image caption generation models. In *Proceedings of the IEEE/CVF Conference on Computer Vision and Pattern Recognition*, pp. 15365–15374, 2022b.
- Simin Chen, Hanlin Chen, Mirazul Haque, Cong Liu, and Wei Yang. The dark side of dynamic routing neural networks: Towards efficiency backdoor injection. In *Proceedings of the IEEE/CVF Conference on Computer Vision and Pattern Recognition*, pp. 24585–24594, 2023.
- An-Chieh Cheng, Hongxu Yin, Yang Fu, Qiushan Guo, Ruihan Yang, Jan Kautz, Xiaolong Wang, and Sifei Liu. Spatialrept: Grounded spatial reasoning in vision-language models. *Advances in Neural Information Processing Systems*, 37:135062–135093, 2024.
- Wei-Lin Chiang, Zhuohan Li, Ziqing Lin, Ying Sheng, Zhanghao Wu, Hao Zhang, Lianmin Zheng, Siyuan Zhuang, Yonghao Zhuang, Joseph E Gonzalez, et al. Vicuna: An open-source chatbot impressing gpt-4 with 90%* chatgpt quality. *See https://vicuna. lmsys. org (accessed 14 April 2023)*, 2(3):6, 2023.
- Wenliang Dai, Junnan Li, Dongxu Li, Anthony Tiong, Junqi Zhao, Weisheng Wang, Boyang Li, Pascale N Fung, and Steven Hoi. Instructblip: Towards general-purpose vision-language models with instruction tuning. *Advances in neural information processing systems*, 36:49250–49267, 2023.

- Jianshuo Dong, Ziyuan Zhang, Qingjie Zhang, Tianwei Zhang, Hao Wang, Hewu Li, Qi Li, Chao Zhang, Ke Xu, and Han Qiu. An engorgio prompt makes large language model babble on. *arXiv* preprint arXiv:2412.19394, 2024.
- Kuofeng Gao, Yang Bai, Jindong Gu, Shu-Tao Xia, Philip Torr, Zhifeng Li, and Wei Liu. Inducing high energy-latency of large vision-language models with verbose images. *arXiv* preprint *arXiv*:2401.11170, 2024a.
- Kuofeng Gao, Jindong Gu, Yang Bai, Shu-Tao Xia, Philip Torr, Wei Liu, and Zhifeng Li. Energy-latency manipulation of multi-modal large language models via verbose samples. arXiv preprint arXiv:2404.16557, 2024b.
- Kaiming He, Xiangyu Zhang, Shaoqing Ren, and Jian Sun. Deep residual learning for image recognition. In *Proceedings of the IEEE conference on computer vision and pattern recognition*, pp. 770–778, 2016.
- Sanghyun Hong, Yiğitcan Kaya, Ionuţ-Vlad Modoranu, and Tudor Dumitraş. A panda? no, it's a sloth: Slowdown attacks on adaptive multi-exit neural network inference. arXiv preprint arXiv:2010.02432, 2020.
- Andrew G Howard, Menglong Zhu, Bo Chen, Dmitry Kalenichenko, Weijun Wang, Tobias Weyand, Marco Andreetto, and Hartwig Adam. Mobilenets: Efficient convolutional neural networks for mobile vision applications. *arXiv preprint arXiv:1704.04861*, 2017.
- Gao Huang, Zhuang Liu, Laurens Van Der Maaten, and Kilian Q Weinberger. Densely connected convolutional networks. In *Proceedings of the IEEE conference on computer vision and pattern recognition*, pp. 4700–4708, 2017.
- Chao Jia, Yinfei Yang, Ye Xia, Yi-Ting Chen, Zarana Parekh, Hieu Pham, Quoc Le, Yun-Hsuan Sung, Zhen Li, and Tom Duerig. Scaling up visual and vision-language representation learning with noisy text supervision. In *International conference on machine learning*, pp. 4904–4916. PMLR. 2021.
- Junnan Li, Dongxu Li, Caiming Xiong, and Steven Hoi. Blip: Bootstrapping language-image pretraining for unified vision-language understanding and generation. In *International conference on machine learning*, pp. 12888–12900. PMLR, 2022.
- Junnan Li, Dongxu Li, Silvio Savarese, and Steven Hoi. Blip-2: Bootstrapping language-image pre-training with frozen image encoders and large language models. In *International conference on machine learning*, pp. 19730–19742. PMLR, 2023.
- Han Liu, Yuhao Wu, Zhiyuan Yu, Yevgeniy Vorobeychik, and Ning Zhang. Slowlidar: Increasing the latency of lidar-based detection using adversarial examples. In *Proceedings of the IEEE/CVF Conference on Computer Vision and Pattern Recognition*, pp. 5146–5155, 2023a.
- Haotian Liu, Chunyuan Li, Qingyang Wu, and Yong Jae Lee. Visual instruction tuning. *Advances in neural information processing systems*, 36:34892–34916, 2023b.
- Alec Radford, Jong Wook Kim, Chris Hallacy, Aditya Ramesh, Gabriel Goh, Sandhini Agarwal, Girish Sastry, Amanda Askell, Pamela Mishkin, Jack Clark, et al. Learning transferable visual models from natural language supervision. In *International conference on machine learning*, pp. 8748–8763. PmLR, 2021.
- Ilia Shumailov, Yiren Zhao, Daniel Bates, Nicolas Papernot, Robert Mullins, and Ross Anderson. Sponge examples: Energy-latency attacks on neural networks. In 2021 IEEE European symposium on security and privacy (EuroS&P), pp. 212–231. IEEE, 2021.
- Hugo Touvron, Thibaut Lavril, Gautier Izacard, Xavier Martinet, Marie-Anne Lachaux, Timothée Lacroix, Baptiste Rozière, Naman Goyal, Eric Hambro, Faisal Azhar, et al. Llama: Open and efficient foundation language models. *arXiv preprint arXiv:2302.13971*, 2023.
- Peng Wang, Shuai Bai, Sinan Tan, Shijie Wang, Zhihao Fan, Jinze Bai, Keqin Chen, Xuejing Liu, Jialin Wang, Wenbin Ge, et al. Qwen2-vl: Enhancing vision-language model's perception of the world at any resolution. *arXiv preprint arXiv:2409.12191*, 2024.

- Zirui Wang, Jiahui Yu, Adams Wei Yu, Zihang Dai, Yulia Tsvetkov, and Yuan Cao. Simvlm: Simple visual language model pretraining with weak supervision. *arXiv preprint arXiv:2108.10904*, 2021.
- Shukang Yin, Chaoyou Fu, Sirui Zhao, Ke Li, Xing Sun, Tong Xu, and Enhong Chen. A survey on multimodal large language models. *National Science Review*, 11(12):nwae403, 2024.
- Jingyi Zhang, Jiaxing Huang, Sheng Jin, and Shijian Lu. Vision-language models for vision tasks: A survey. *IEEE transactions on pattern analysis and machine intelligence*, 46(8):5625–5644, 2024a.
- Susan Zhang, Stephen Roller, Naman Goyal, Mikel Artetxe, Moya Chen, Shuohui Chen, Christopher Dewan, Mona Diab, Xian Li, Xi Victoria Lin, et al. Opt: Open pre-trained transformer language models. *arXiv preprint arXiv:2205.01068*, 2022.
- Yuanhe Zhang, Zhenhong Zhou, Wei Zhang, Xinyue Wang, Xiaojun Jia, Yang Liu, and Sen Su. Crabs: Consuming resource via auto-generation for llm-dos attack under black-box settings. *arXiv* preprint arXiv:2412.13879, 2024b.
- Deyao Zhu, Jun Chen, Xiaoqian Shen, Xiang Li, and Mohamed Elhoseiny. Minigpt-4: Enhancing vision-language understanding with advanced large language models. *arXiv preprint arXiv:2304.10592*, 2023.

Appendix

A USE OF LARGE LANGUAGE MODELS

In this study, large language models were used solely to polish the manuscript text, improving the fluency and clarity of the writing.

B EXPERIMENTAL DETAILS

The conversational template used by LLaVA and Qwen2-VL is as follows:

C ADDITIONAL EXPERIMENTS

Figure 5 presents the token-length distributions of original images and adversarial images across four models. For all four models, the token lengths of original images are concentrated toward the left, whereas those of adversarial images cluster on the far right. Meanwhile, due to model-specific characteristics, LLAVA and Qwen2-VL generate more tokens than BLIP2 and InstructBLIP on original images, and their distributions are close to Gaussian.

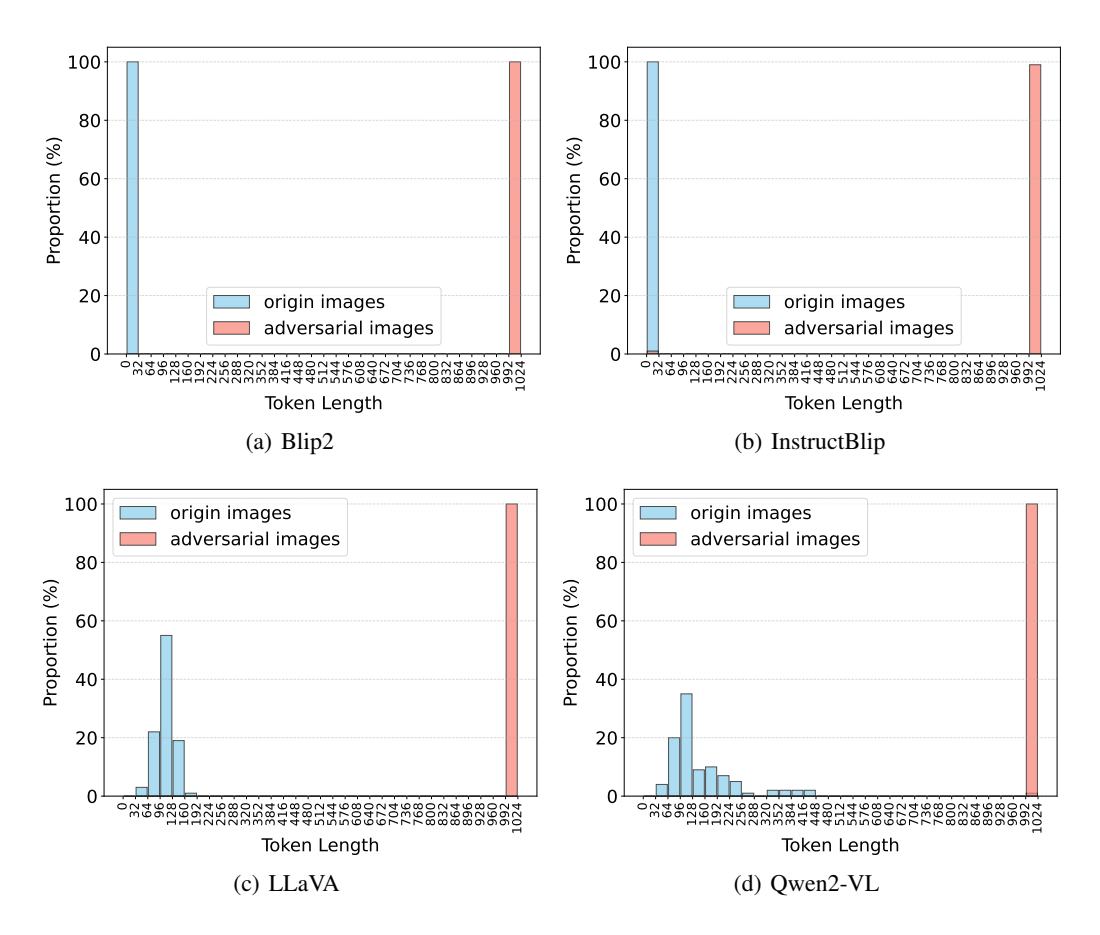


Figure 5: The token-length distribution of original images and adversarial images across the four models.